International Journal of Thermophysics, Vol. 12, No. 4, 1991

Thermal Expansion of TiAl + TiB_2 Alloys and Model Calculations of Stresses and Expansion of Continuous Fiber Composites[1]

T. A. Hahn[2]

Thermal expansion values for three TiAl alloys with different additions of TiB_2 can be represented using a third-order equation at temperatures between 20 and 800°C. Expansion values were obtained on both heating and cooling temperature cycles. The total expansion at 800°C is between 0.917 and 0.931% for three different samples. The expansivity increases from about 10×10^{-6} °C^{-1} at 80°C to 14×10^{-6} °C^{-1} at 750°C. A five-coaxial cylinder elastic model for multizone-coated continuous fiber composites is developed for predicting stresses and thermal expansion of composites. Either isotropic or transversely isotropic material properties can be assigned to the various cylinder zones.

KEY WORDS: continuous fiber composites; stress/strain calculations; thermal expansion; TiAl + TiB_2 alloys.

1. INTRODUCTION

In recent developments of titanium aluminide alloys for high-temperature aerospace applications, materials have been fabricated that possess greater toughness and creep resistance than the parent aluminide. The termal expansion characteristics of these alloys are needed to provide input data for calculating the thermomechanical response of composites using these alloys as matrix materials. TiAl reacts with both graphite and silicon

[1] Paper presented at the Tenth International Thermal Expansion Symposium, June 6–7, 1989, Boulder, Colorado, U.S.A.

[2] Composites and Ceramics Branch, Naval Research Laboratory, Washington, D.C. 20375, U.S.A.

0195-928X/91/0700-0711$06.50/0

carbide fibers, resulting in brittle reaction zones. For this reason, it has been proposed that the fibers first be coated to prevent or slow the interaction. Multiple-barrier coatings, as well as the TiAl alloy, can be coated directly onto the fibers, which can then be consolidated into the final composite. In order to calculate the thermomechanical response of such an ensemble as a function of temperature or mechanical loading, a five-coaxial cylinder model has been developed. This model is based on solving the constants in the displacement equations using the equality of the displacements and stresses at the interfaces between the coaxial cylinders and the balance of axial forces. These constants can then be used to calculate the internal stresses and overall deformation and thermal expansion of the composite.

Results of the thermal expansion measurements are presented for three TiAl alloys over the temperature range from 20 to 800°C. Model predictions of the internal stresses for a SiC–TiAl composite are compared to the stresses calculated with the addition of a 2-μm amorphous carbon coating or a 2-μm TiB_2 coating between the fiber and the matrix. In addition, the stresses are calculated when both of the coatings are applied to the fiber and an infinite composite, with volume-averaged material properties, surrounds the fiber, coatings, matrix combination. Predicted thermal expansivity values are reported for both the SiC fiber composites and a graphite fiber composite.

2. THERMAL EXPANSION OF TiAl + TiB_2 ALLOYS

Thermal expansion measurements were carried out on three separate experimental TiAl alloys manufactured by the Martin Marietta Laboratories in a high-temperature aerospace materials development program. The alloys were produced using a proprietary XD process to incorporate TiB_2 ceramic particles in the TiAl intermetallic matrix. Samples from three different ingots were tested. The nominal composition of each ingot is as follows: Ingot 16, Ti–44 at% Al + 5 vol% TiB_2; Ingot 17, Ti–46 at% Al–2 at% V + 6.6 vol% TiB_2; and Ingot 2, Ti–40 at% Al + 9 vol% TiB_2.

The measurements were performed using a fused quartz dilatometer with corrections determined by comparison of the measurements on a pure platinum sample with reported expansion values [1]. Length measurements were made at equilibrium temperatures extending from room temperature to 800°C at every hundred degree value on both heating and cooling.

The averaged expansion values for each sample, which were obtained from two-, three-, and four-measurement cycles, were combined to obtain

a least-squares fit to a third-order polynomial equation to represent the data. The resulting equation for the percentage expansion from 20°C is

$$\Delta L/L_{20}\,(\%) = -1.9808 \times 10^{-2} + 9.85604 \times 10^{-4}\,T + 2.18104 \times 10^{-7}\,T^2 + 2.90545 \times 10^{-11}\,T^3 \quad (1)$$

The data from two of the samples exhibited small systematic departure from this equation, but all the data were within 1% of the values predicted from the equation. The departure of the averaged data from each of the samples is shown in Fig. 1. Expansivity values from the derivative of Eq. (1) are within 2% of the values derived from the experimental data.

3. MODEL DEVELOPMENT

The five-coaxial cylinder ensemble, consisting of a fiber, two coatings, the matrix, and the surrounding composite, is shown in Fig. 2 along with the various radii used in the analysis. A solution technique using cylindrical coordinates (r, θ, z) developed by Mikata and Taya [2] for a four-cylinder ensemble has been extended to include five coaxial cylinders. End effects are neglected and isothermal temperatures are assumed with no radially or axially temperature gradients. The solution also allows for axial or radial applied stresses.

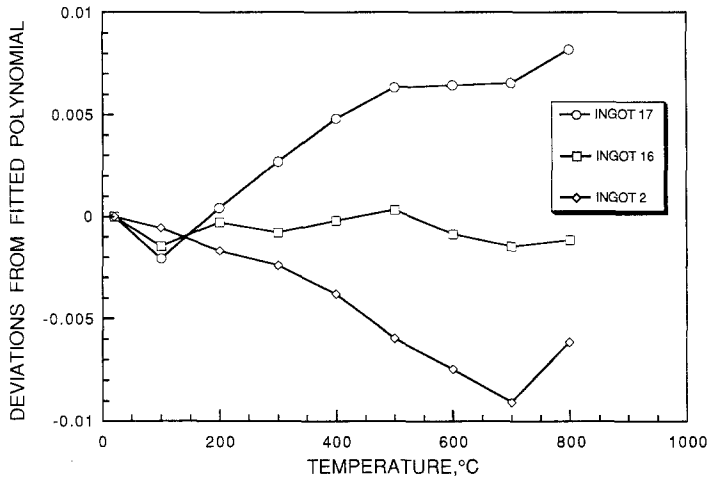

Fig. 1. Deviations of the expansion for three $TiAl + TiB_2$ alloys from the least-squares fitted equation.

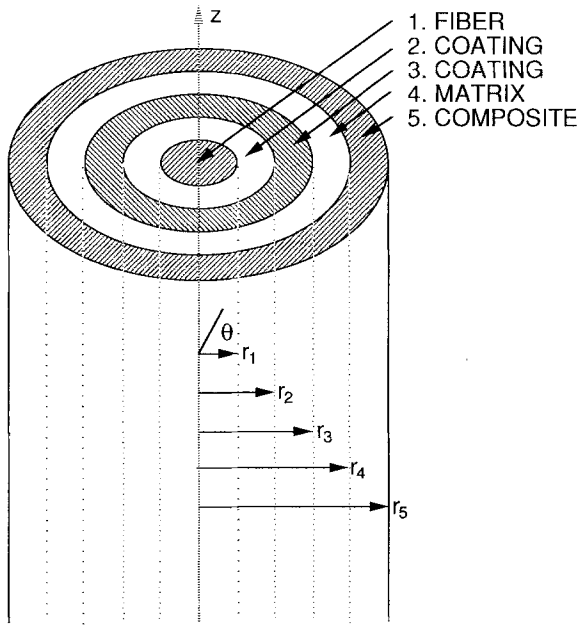

Fig. 2. Five coaxial cylinders model for a coated fiber composite.

Following the development of Mikata and Taya for cylindrical symmetry, the stress (σ)–strain (e) equations are

$$\begin{aligned}
\sigma_{rr}^{(n)} &= C_{11}^{(n)} e_{rr}^{(n)} + C_{12}^{(n)} e_{\theta\theta}^{(n)} + C_{13}^{(n)} e_{zz}^{(n)} - \beta_1^{(n)} T_n \\
\sigma_{\theta\theta}^{(n)} &= C_{12}^{(n)} e_{rr}^{(n)} + C_{11}^{(n)} e_{\theta\theta}^{(n)} + C_{13}^{(n)} e_{zz}^{(n)} - \beta_1^{(n)} T_n \\
\sigma_{zz}^{(n)} &= C_{13}^{(n)} e_{rr}^{(n)} + C_{13}^{(n)} e_{\theta\theta}^{(n)} + C_{33}^{(n)} e_{zz}^{(n)} - \beta_3^{(n)} T_n
\end{aligned} \tag{2}$$

where superscript (n) refers to cylinders 1–5, the subscripts refer to the directions, C_{ij} are the elastic constants, T_n is the temperature of cylinder (n), and

$$\begin{aligned}
\beta_1^{(n)} &= [C_{11}^{(n)} + C_{12}^{(n)}]\, \alpha_1^{(n)} + C_{13}^{(n)} \alpha_3^{(n)} \\
\beta_3^{(n)} &= 2C_{13}^{(n)} \alpha_1^{(n)} + C_{33}^{(n)} \alpha_3^{(n)}
\end{aligned} \tag{3}$$

where $\alpha_1^{(n)}$ and $\alpha_3^{(n)}$ are the coefficients of thermal expansion of cylinder zone (n) in the transverse and longitudinal directions respectively. Due to

the axisymmetry, the strains in terms of the radial displacement u and axial displacement w are

$$e_{rr}^{(n)} = \frac{\partial u_n}{\partial r}$$

$$e_{\theta\theta}^{(n)} = \frac{u_n}{r} \tag{4}$$

$$e_{zz}^{(n)} = \frac{\partial w_n}{\partial z}$$

where u is a function of r and w is a function of z. Substitution of Eqs. (4) into Eqs. (3) gives the displacement equations as

$$\sigma_{rr}^{(n)} = C_{11}^{(n)} \frac{\partial u_n}{\partial r} + C_{12}^{(n)} \frac{u_n}{r} + C_{13}^{(n)} \frac{\partial w_n}{\partial z} - \beta_1^{(n)} T_n$$

$$\sigma_{\theta\theta}^{(n)} = C_{12}^{(n)} \frac{\partial u_n}{\partial r} + C_{11}^{(n)} \frac{u_n}{r} + C_{13}^{(n)} \frac{\partial w_n}{\partial z} - \beta_1^{(n)} T_n \tag{5}$$

$$\sigma_{zz}^{(n)} = C_{13}^{(n)} \frac{\partial u_n}{\partial r} + C_{13}^{(n)} \frac{u_n}{r} + C_{33}^{(n)} \frac{\partial w_n}{\partial z} - \beta_3^{(n)} T_n$$

For isothermal temperatures the equilibrium equations give the displacements as

$$\frac{d^2 u_n}{dr^2} + \frac{1}{r}\frac{du_n}{dr} - \frac{u_n}{r^2} = 0$$

$$\frac{d^2 w_n}{dz^2} = 0 \tag{6}$$

which have the general solutions

$$u_n(r) = A_n r + \frac{B_n}{r}$$

$$w_n(z) = G_n z + H_n \tag{7}$$

From the equality of axial displacement in each cylinder

$$G_1 = \cdots = G_5 = G$$

$$H_1 = \cdots = H_5 = H \tag{8}$$

H can be seen to be just a rigid-body displacement in the axial direction which can be set equal to zero. Substitution into the stress displacement Eqs. (5) gives

$$\sigma_{rr}^{(n)} = C_{11}^{(n)}\left[A_n - \frac{B_n}{r^2}\right] + C_{12}^{(n)}\left[A_n + \frac{B_n}{r^2}\right] + C_{13}^{(n)}G - \beta_1^{(n)}T_n$$

$$\sigma_{\theta\theta}^{(n)} = C_{12}^{(n)}\left[A_n - \frac{B_n}{r^2}\right] + C_{11}^{(n)}\left[A_n + \frac{B_n}{r^2}\right] + C_{13}^{(n)}G - \beta_1^{(n)}T_n \tag{9}$$

$$\sigma_{zz}^{(n)} = 2C_{13}^{(n)}A_n + C_{33}^{(n)}G - \beta_3^{(n)}T_n$$

where the constants A_n, B_n, and G will be determined by the boundary conditions. For the five-cylinder model these boundary conditions are

$$\begin{aligned}
&u_1 = u_2, \quad && w_1 = w_2, \quad && \sigma_{rr}^{(1)} = \sigma_{rr}^{(2)} \quad && \text{at} \quad r = r_1 \\
&u_2 = u_3, \quad && w_2 = w_3, \quad && \sigma_{rr}^{(2)} = \sigma_{rr}^{(3)} \quad && \text{at} \quad r = r_2 \\
&u_3 = u_4, \quad && w_3 = w_4, \quad && \sigma_{rr}^{(3)} = \sigma_{rr}^{(4)} \quad && \text{at} \quad r = r_3 \\
&u_4 = u_5, \quad && w_4 = w_5, \quad && \sigma_{rr}^{(4)} = \sigma_{rr}^{(5)} \quad && \text{at} \quad r = r_4 \\
& && && \sigma_{rr}^{(5)} = \sigma_{0r} \quad && \text{at} \quad r = r_5
\end{aligned} \tag{10}$$

where σ_{0r} is the applied radial stress.

In addition, the balance of axial forces is

$$\int_0^{r_1} \sigma_{zz}^{(1)}\, r\, dr + \cdots + \int_{r_4}^{r_5} \sigma_{zz}^{(5)}\, r\, dr = \int_0^{r_5} \sigma_{0z}\, r\, dr \tag{11}$$

where σ_{0z} is the applied stress in the z direction.

Substitution of the stress–strain equations in the boundary condition equations and the balance of forces equation gives a set of linear equations for the unknown parameters A_n, B_n, and G. These equations can be represented by the following matrix equation.

$$\begin{bmatrix}
a_{11} & a_{12} & a_{13} & 0 & 0 & 0 & 0 & 0 & 0 & 0 \\
0 & a_{22} & a_{23} & a_{24} & a_{25} & 0 & 0 & 0 & 0 & 0 \\
0 & 0 & 0 & a_{34} & a_{35} & a_{36} & a_{37} & 0 & 0 & 0 \\
0 & 0 & 0 & 0 & 0 & a_{46} & a_{47} & a_{48} & a_{49} & 0 \\
a_{51} & a_{52} & a_{53} & 0 & 0 & 0 & 0 & 0 & 0 & a_{510} \\
0 & a_{62} & a_{63} & a_{64} & a_{65} & 0 & 0 & 0 & 0 & a_{610} \\
0 & 0 & 0 & a_{74} & a_{75} & a_{76} & a_{77} & 0 & 0 & a_{710} \\
0 & 0 & 0 & 0 & 0 & a_{86} & a_{87} & a_{88} & a_{89} & a_{810} \\
0 & 0 & 0 & 0 & 0 & 0 & 0 & a_{98} & a_{99} & a_{910} \\
a_{101} & a_{102} & 0 & a_{104} & 0 & a_{106} & 0 & a_{108} & 0 & a_{1010}
\end{bmatrix}
\begin{bmatrix} A_1 \\ A_2 \\ B_2 \\ A_3 \\ B_3 \\ A_4 \\ B_4 \\ A_5 \\ B_5 \\ G \end{bmatrix}
=
\begin{bmatrix} 0 \\ 0 \\ 0 \\ 0 \\ c_5 \\ c_6 \\ c_7 \\ c_8 \\ c_9 \\ c_{10} \end{bmatrix} \tag{12}$$

The individual a_{ij} and c_j are listed in the Appendix. Since A_n, B_n, and G are dependent on the various radii, which in turn are dependent on the temperature, these also will be dependent on the temperature. This dependency, however, is small and, for large temperature changes, can be adjusted for by substitution of new radii when necessary. In case the materials are isotropic the stiffness constants reduce to

$$C_{11}^{(n)} = C_{33}^{(n)} = 2\mu_n + \lambda_n = \frac{(1-\nu_n)E_n}{(1+\nu_n)(1-2\nu_n)}$$

$$C_{12}^{(n)} = C_{13}^{(n)} = \lambda_n = \frac{\nu_n E_n}{(1+\nu_n)(1-2\nu_n)} \tag{13}$$

$$\beta_1^{(n)} = \beta_3^{(n)} = (2\mu_n + 3\lambda_n)\,\alpha_1^{(n)} = \frac{E_n \alpha_1^{(n)}}{(1-2\nu_n)}$$

where, for material in cylinder $n = 1 \cdots 5$, μ_n and λ_n are the Lame constants, ν_n are the Poisson's ratios, and E_n are the Young's moduli. After calculating the constants in Eq. (12), the stresses are calculated using Eq. (9), and the displacements from Eq. (7). The expansivity is calculated by dividing the strain in Eq. (4) by the change in temperature.

4. STRESS/STRAIN CALCULATIONS

Stress calculations have been carried out for the case of a SiC fiber coated with C and/or TiB_2, a TiAl matrix, and a surrounding composite having the volume-averaged properties of the other materials in the composite. The material properties used in the calculations are shown in Table I. A fiber volume fraction of approximately 0.20 was used in the calculations. The radius of the fiber equaled 70 μm and that of the matrix was 156.5 μm. The thickness of the C and TiB_2 coatings was 2.0 μm. The composite radius was set equal to 1.0 m to simulate a large composite. With this large radius of the surrounding composite, the axial force balance was taken only across the fiber, coatings, and matrix.

Figure 3 shows the calculated stresses at the outer fiber radius and

Table I. Material Properties

	SiC	TiAl	C	TiB_2
E (GPa)	427	175	20	473
ν	0.30	0.30	0.20	0.32
α (10^{-6} °C^{-1})	3.3	10	3.5	5.6

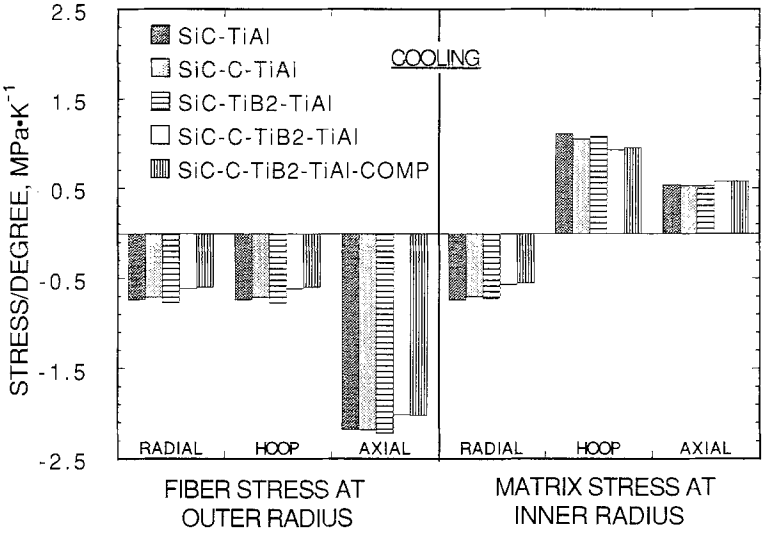

Fig. 3. Fiber and matrix stresses calculated from the coaxial cylinders model for a temperature change of $-1°C$.

matrix stresses at the inner matrix radius for a SiC fiber–TiAl matrix composite. When fewer than five cylinders are being considered, the same material properties are assigned to contiguous cylinder zones. The first case considered was a two-cylinder composite consisting of the SiC fiber and the TiAl matrix; then the effects of either a C coating or a TiB_2 coating were considered. Next calculations were carried out for both coatings between the fiber and the matrix. Finally, the effects of an outer composite zone were calculated using the volume-averaged material properties of the four inner zones. The stresses are directly proportional to the temperature changes, so in order to simulate the stresses after a high-temperature processing, a temperature change of $-1°C$ was used in the calculations. The calculations were carried out assuming zero applied radial and axial stress. Since the stresses are directly proportional to the temperature change, the individual stresses would reverse sign upon heating.

For cooling, all the stresses in the fiber are compressive. The addition of the C coating between the fiber and the matrix reduces the radial and hoop stress in the fiber, while the axial stress is not affected when compared to the composite with no fiber coating. In contrast, the TiB_2 coating increases all the stresses in the fiber when compared to the uncoated fiber composite. With the addition of both the C and the TiB_2 coatings, all three stresses in the fiber are reduced below that of the uncoated fiber composite and either the C- or the TiB_2-coated fiber composite. The addition of the

composite as the outer cylinder further reduces the radial and hoop stresses, while the axial stress is not altered because the force balance is only considered across the inner four cylinders.

The matrix stresses, at the inner matrix radius, have qualitatively similar behavior with the addition of the coatings and outer composite cylinders. The radial stresses are compressive for all the composites and the hoop and axial stresses are tensile. With the addition of the C coating, all three matrix stresses are reduced when compared to the uncoated fiber composite. With the TiB_2 coating, the radial and hoop stresses are greater than with the C coating, but all three matrix stresses are less than with the uncoated fiber composite. With the addition of both the C and the TiB_2 coatings, the radial and hoop stresses are less than the uncoated fiber composite and less than with either the C- or the TiB_2-coated fiber composites. The axial stress is increased over the three previous composites. The addition of the composite as the outer cylinder reduces the radial stress to its smallest value but increases the hoop stress as compared to either the C- or the TiB_2-coated fiber composite; however, it is less than the uncoated and either the C- or the TiB_2-coated fiber composite. The axial stress is, again, as in the fiber, essentially equal to the value when no composite is present because of the force balance being only across the four inner cylinders.

In all of the model calculations the maximum matrix stresses were always at the inner matrix radius so that matrix yielding or failure would be initiated at the inner matrix radius. Using an ultimate stress of 970 MPa for the TiAl matrix and the effective stress calculated from

$$\sigma_e = \frac{1}{\sqrt{2}} \sqrt{\sum (\sigma_{ii} - \sigma_{jj})^2} \tag{14}$$

the addition of the combined C and TiB_2 coatings increases the temperature change to reach the ultimate stress by approximately 100°C when compared to the uncoated fiber matrix composite.

Figure 4 shows the predicted radial and axial expansivities for a C- and TiB_2-coated SiC fiber TiAl matrix four-coaxial cylinder composite as a function of the matrix volume fraction. Also shown are the calculated expansivities for a transversely isotropic graphite fiber composite with the same coatings and matrix. In the case of the isotropic SiC fiber the predicted axial and radial expansivities are near the linear rule of mixtures, which is a straight line between the expansivities of SiC and TiAl. The radial expansivity is slightly greater than the linear rule of mixtures and the axial expansivity is slightly less than the linear rule of mixtures. The calculated expansivities for the graphite fiber composites demonstrates the model's

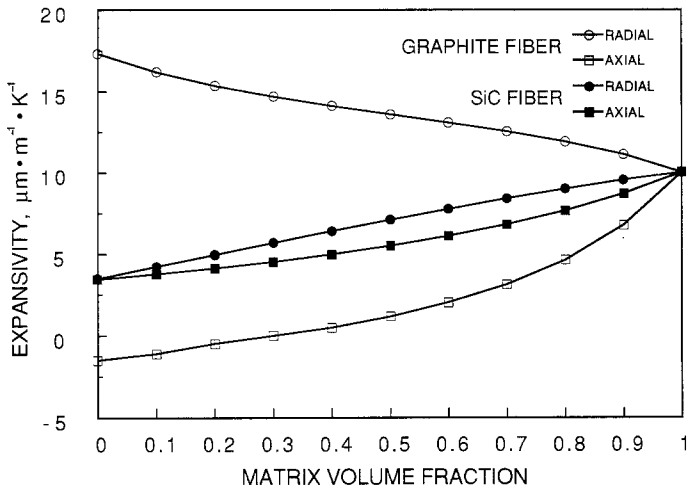

Fig. 4. Predicted radial and axial expansivities for C- and TiB_2-coated SiC and graphite fiber with a TiAl matrix using the four-coaxial cylinder model.

capabilities for incorporating transversely isotropic materials in the calculations. For these calculations, the axial modulus of the fiber is assumed to be 690 GPa, the transverse modulus 14 GPa, the axial expansivity $-1.5 \times 10^{-6}\ °C^{-1}$, and the transverse expansivity $18 \times 10^{-6}\ °C^{-1}$. The radial expansivity decreases from a value for the coated fiber to the matrix value, while the axial expansivity increases from the value for the coated fiber to the matrix value as the matrix volume fraction varies from 0 to 1.

5. CONCLUSIONS

Thermal expansion values of three $TiAl + TiB_2$ alloys can be represented to within approximately 1% by a third-order polynomial equation. Deviations of the expansion values for the three samples have been presented so that the expansion values for any of the samples could be calculated for more accurate data. Stress values from the five coaxial cylinder model can be calculated for two to five coaxial cylinders. For cooling, the fiber stresses are compressive for the matrix-coated fiber as well as with the addition of the fiber coatings and outer composite. The addition of the coatings reduces the stresses in the fiber when compared to the uncoated fiber matrix composite. In the case of the matrix stresses at the inner matrix radius, the radial stress is compressive while the hoop and axial stresses are tensile. All the stresses remain of the same sign with the addition of the coatings and the outer composite. The compressive

radial stress and tensile hoop stress decrease in magnitude with the addition of the two coatings. The axial stress in the matrix is tensile and increases with the addition of the two coatings as compared to the uncoated fiber matrix composite. However, the addition of the two fiber coatings reduces the effective stress so that the composite could be subjected to a greater temperature change before the effective stress reaches the ultimate tensile stress of the matrix material.

APPENDIX

$$a_{11} = r_1 \qquad a_{35} = \frac{1}{r_3} \qquad a_{51} = C_{11}^{(1)} + C_{12}^{(1)} \qquad a_{62} = C_{11}^{(2)} + C_{12}^{(2)}$$

$$a_{12} = -r_1 \qquad a_{36} = -r_3 \qquad a_{52} = -C_{11}^{(2)} - C_{12}^{(2)} \qquad a_{63} = \frac{C_{12}^{(2)} - C_{11}^{(2)}}{r_2^2}$$

$$a_{13} = -\frac{1}{r_1} \qquad a_{37} = -\frac{1}{r_3} \qquad a_{53} = \frac{C_{11}^{(1)} - C_{12}^{(1)}}{r_1^2} \qquad a_{64} = -C_{11}^{(3)} - C_{12}^{(3)}$$

$$a_{22} = r_2 \qquad a_{46} = r_4 \qquad a_{510} = C_{13}^{(1)} - C_{13}^{(2)} \qquad a_{65} = \frac{C_{11}^{(3)} - C_{12}^{(3)}}{r_2^2}$$

$$a_{23} = \frac{1}{r_2} \qquad a_{47} = \frac{1}{r_4} \qquad\qquad a_{610} = C_{13}^{(2)} - C_{13}^{(3)}$$

$$a_{24} = -r_2 \qquad a_{48} = -r_4$$

$$a_{25} = -\frac{1}{r_2} \qquad a_{49} = -\frac{1}{r_4}$$

$$a_{34} = r_3$$

$$a_{74} = C_{11}^{(3)} + C_{12}^{(3)} \qquad a_{86} = C_{11}^{(4)} + C_{12}^{(4)} \qquad a_{98} = C_{11}^{(5)} + C_{12}^{(5)}$$

$$a_{75} = \frac{C_{12}^{(3)} - C_{11}^{(3)}}{r_3^2} \qquad a_{87} = \frac{C_{12}^{(4)} - C_{11}^{(4)}}{r_4^2} \qquad a_{99} = \frac{C_{12}^{(5)} - C_{11}^{(5)}}{r_5^2}$$

$$a_{76} = -C_{11}^{(4)} - C_{12}^{(4)} \qquad a_{88} = -C_{11}^{(5)} - C_{12}^{(5)} \qquad a_{910} = C_{13}^{(5)}$$

$$a_{77} = \frac{C_{11}^{(4)} - C_{12}^{(4)}}{r_3^2} \qquad a_{89} = \frac{C_{11}^{(5)} - C_{12}^{(5)}}{r_4^2} \qquad a_{101} = 2C_{13}^{(1)} r_1^2$$

$$a_{710} = C_{13}^{(3)} - C_{13}^{(4)} \qquad a_{810} = C_{13}^{(4)} - C_{13}^{(5)} \qquad a_{102} = 2C_{13}^{(2)}(r_2^2 - r_1^2)$$

$$a_{104} = 2C_{13}^{(3)}(r_3^2 - r_2^2)$$
$$a_{106} = 2C_{13}^{(4)}(r_4^2 - r_3^2)$$
$$a_{108} = 2C_{13}^{(5)}(r_5^2 - r_4^2)$$
$$a_{1010} = C_{33}^{(1)}r_1^2 + C_{33}^{(2)}(r_2^2 - r_1^2) + C_{33}^{(3)}(r_3^2 - r_2^2) + C_{33}^{(4)}(r_4^2 - r_3^2) + C_{33}^{(5)}(r_5^2 - r_4^2)$$

$$c_5 = (\beta_1^{(1)} - \beta_1^{(2)})\,\Delta T \qquad c_9 = \sigma_{0r} + \beta_1^{(5)}\,\Delta T$$
$$c_6 = (\beta_1^{(2)} - \beta_1^{(3)})\,\Delta T \qquad c_{10} = \beta_3^{(1)}r_1^2 + \beta_3^{(2)}\,\Delta T(r_2^2 - r_1^2) + \beta_3^{(3)}\,\Delta T(r_3^2 - r_2^2)$$
$$c_7 = (\beta_1^{(3)} - \beta_1^{(4)})\,\Delta T \qquad + \beta_3^{(4)}\,\Delta T(r_4^2 - r_3^2) + \beta_3^{(5)}\,\Delta T(r_5^2 - r_4^2) + \sigma_{oz}r_5^2$$
$$c_8 = (\beta_1^{(4)} - \beta_1^{(5)})\,\Delta T$$

REFERENCES

1. T. A. Hahn and R. K. Kirby, in *Thermal Expansion—1971*, Am. Inst. Phys. Conf. Proc. No. 3, M. G. Graham and H. E. Hagy, eds., H. C. Wolfe, series ed. (Am. Inst. Phys., New York, 1972), p. 87.
2. Y. Mikata and M. Taya, *J. Comp. Mater.* **19**:554 (1985).